Bonding Analysis

Deutsche Ausgabe: DOI: 10.1002/ange.201904546
Internationale Ausgabe: DOI: 10.1002/anie.201904546

M–O Bonding Beyond the Oxo Wall: Spectroscopy and Reactivity of Cobalt(III)-Oxyl and Cobalt(III)-Oxo Complexes

Erik Andris, Rafael Navrátil, Juraj Jašík, Martin Srnec, Mònica Rodríguez, Miquel Costas* und Jana Roithová**

Abstract: *Terminal oxo complexes of late transition metals are frequently proposed reactive intermediates. However, they are scarcely known beyond Group 8. Using mass spectrometry, we prepared and characterized two such complexes: $[(N4Py)Co^{III}(O)]^+$ (**1**) and $[(N4Py)Co^{IV}(O)]^{2+}$ (**2**). Infrared photodissociation spectroscopy revealed that the Co–O bond in **1** is rather strong, in accordance with its lack of chemical reactivity. On the contrary, **2** has a very weak Co–O bond characterized by a stretching frequency of $\leq 659\ cm^{-1}$. Accordingly, **2** can abstract hydrogen atoms from non-activated secondary alkanes. Previously, this reactivity has only been observed in the gas phase for small, coordinatively unsaturated metal complexes. Multireference ab-initio calculations suggest that **2**, formally a cobalt(IV)-oxo complex, is best described as cobalt(III)-oxyl. Our results provide important data on changes to metal-oxo bonding behind the oxo wall and show that cobalt-oxo complexes are promising targets for developing highly active C–H oxidation catalysts.*

Introduction

The terminal oxo ligand is a strong π donor that can form metal-oxo triple bonds with early transition metals such as in $V{\equiv}O^{2+}$ or $Mo{\equiv}O^{3+}$.[1,2] When progressing to late transition metals, the occupancy of π-antibonding metal d orbitals increases, and metal-oxo bonds become weaker and more reactive. This culminates in the rich chemistry of iron-oxo compounds, such as heme (P450)[3–5] and non-heme iron enzymes[6,7] that inspired the development of important C–H oxidation catalysts.[8–10] In contrast, metal-oxo complexes beyond Group 8 are rare and exist only in square-pyramidal,[11] trigonal-pyramidal,[12,13] and, importantly, square-planar[14] coordination geometries in which electrons occupy M–O non-bonding (or weakly π^*-antibonding) d orbitals. Stabilization of metal-oxo complexes beyond Group 8 has also been achieved by coordination of oxygen to Lewis acids.[15] Earlier reports of pseudo-octahedral platinum, gold, and palladium complexes were subsequently disproved for incorrect structural assignment.[16]

The sudden change in the abundance of complexes between Group 8 and Group 9 has long been noted[17,18] and is commonly known as the oxo wall.[19–21] However, the oxo-wall postulate does not exclude the possibility that such complexes act as reaction intermediates. Quite the contrary—the complexes behind the oxo wall (Group 9 and beyond) should be exceptionally reactive and their existence has been inferred in numerous oxidation reactions.[21–27]

The molecular orbital theory readily explains this empirically observed oxo wall. Orbital energies in tetragonal oxo complexes follow the order $d_{xy} < d_{xz} = d_{yz} < d_{x^2-y^2} < d_{z^2}$ (M–O bond on the z axis). The d_{xz} and d_{yz} orbitals are π*(M–O) orbitals, therefore the metal-oxo π-bond order drops below one when more than four d electrons are present (Figure 1a), which often occurs beyond Group 8 due to the available oxidation states. Reported square-pyramidal rhenium(I)-oxo[28] and trigonal iron(III)-oxo[29–31] complexes have more than four d electrons, but a different symmetry. The only complex that can be considered to be behind the oxo wall is a cobalt(IV)-oxo complex reported by the Nam group.[11] However, this complex features full Co=O double bond because its square-pyramidal geometry makes the $d_{x^2-y^2}$ orbital energetically accessible.[11] We have recently prepared and characterized gas-phase d^5 tetragonal iron(III)-oxo complexes with an N4Py (*N*,*N*-bis(2-pyridylmethyl)-*N*-bis(2-pyridyl)methylamine) ligand in quartet (Figure 1b) and sextet (Figure 1c) spin states.[32] The quartet-state complex has a Fe=O double bond, whereas the sextet state complex retains the Fe–O π-bond order, but the Fe–O σ bond weakens to an order of one half (Figure 1c). Hence, we aimed to investigate the changes to the metal-oxo bond upon crossing the oxo wall by replacing iron with cobalt.

[*] E. Andris, R. Navrátil, Dr. J. Jašík, Prof. J. Roithová
Department of Organic Chemistry, Faculty of Science
Charles University
Hlavova 2030/8, 128 43 Prague 2 (Czech Republic)
Dr. M. Srnec
J. Heyrovsky Institute of Physical Chemistry of the CAS
v. v. i., Dolejškova 2155/3, 1822 3 Prague 8 (Czech Republic)
E-Mail: martin.srnec@jh-inst.cas.cz
M. Rodríguez, Prof. M. Costas
Departament de Quimica and Institute of Computational Chemistry and Catalysis (IQCC), University of Girona
Campus Montilivi, Girona 17071 (Spain)
E-Mail: miquel.costas@udg.edu
Prof. J. Roithová
Radboud University Nijmegen, Institute for Molecules and Materials
Heyendaalseweg 135, 6525 AJ Nijmegen (The Netherlands)
E-Mail: jana.roithova@ru.nl
Supporting information and the ORCID identification number(s) for the author(s) of this article can be found under: https://doi.org/10.1002/anie.201904546.

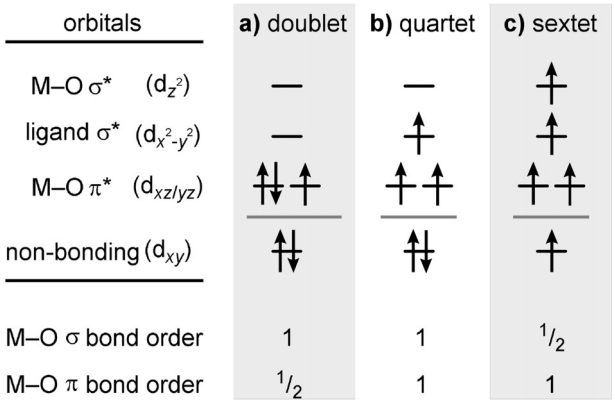

Figure 1. Electronic configuration of tetragonal d^5 metal-oxo complexes in a) doublet, b) quartet, and c) sextet states.

In comparison to analogous iron(III)-oxo complexes, the higher cobalt(IV) oxidation state induces a larger orbital splitting and thus stabilizes the low-spin configuration (Figure 1 a).[33] Furthermore, the energy of the metal d orbitals might in fact be lower than the energy of the oxygen orbitals in cobalt-oxo complexes and thus, cobalt(IV)-oxo might be better described as cobalt(III)-oxyl.[21] Considering the expected extreme reactivity of cobalt(IV)-oxo, we decided to prepare these complexes in the gas phase where they could persist long enough to allow their complete characterization by ion-spectroscopic methods and by ion–molecule reactions.[34–36]

Cryogenic gas-phase ion spectroscopy has inherent advantages to the condensed-phase spectroscopies. First, the ions are isolated in the vacuum and thus unaffected by interactions with other species except one helium atom with negligible effect on its properties.[35] Second, the ions are cooled to only a few K, therefore they are in the ground electronic and vibrational state. Third, the spectra are associated with mass-selected ions, thus eliminating interferences normally present in solution. We can encounter and characterize isomeric ions with the same m/z ratio.[37,38] Such a case was not observed in this study, therefore all reported spectra as well as reactivities herein correspond to single defined species.

Results and Discussion

High-valent gaseous metal-oxo complexes can be prepared from metal-chlorate or nitrate precursors because these precursors eliminate $ClO_2^{\bullet}$ or $NO_2^{\bullet}$ radicals in collisional activation during the transfer to the gas phase.[39,40] We have thus probed this approach for $[(N4Py)Co^{II}(ClO_3)](ClO_3)$.[41] Electrospray ionization of an acetonitrile solution of $[(N4Py)Co^{II}(ClO_3)](ClO_3)$ afforded the desired cobalt complexes $[(N4Py)Co^{II}(ClO_3)]^+$ (m/z 509) and $[(N4Py)Co^{III}(O)]^+$ (**1**; m/z 221; Figure S1 a in the Supporting Information). Furthermore, we electrochemically oxidized the cobalt-chlorate complex in solution using a flow setup (Figure S2), which allowed us to prepare $[(N4Py)Co^{III}(ClO_3)]^{2+}$ (m/z 254.5) and $[(N4Py)Co^{IV}(O)]^{2+}$ (**2**; m/z 221; Figure S1 b). Complexes $[(N4Py)Co^{III}(O)]^+$ (**1**) and $[(N4Py)Co^{IV}(O)]^{2+}$ (**2**) were further studied by helium-tagging infrared and visible photodissociation (IRPD and visPD) spectroscopy,[35] by reactivity probing with hydrocarbons, and by theoretical calculations.

The IRPD spectrum of d^6 cobalt(III)-oxo complex **1** in Figure 2 a shows a ν(Co–O) band at 752 cm^{-1}, which shifts to 718 cm^{-1} upon ^{18}O labeling, consistent with the ν(Co–O) assignment. The position of this band is similar to that of analogous sextet iron(III)-oxo complexes,[32] 63 cm^{-1} lower than the ν(Co–O) band in the trigonal singlet cobalt(III)-oxo complex reported by Goetz et al.[12] and 18 cm^{-1} lower than the ν(Co–O) band in the quartet cobalt(IV)-oxo complex reported by Wang et al.[11] The ν(Co–O) frequency thus indicates that the Co–O bond order is less than two. Furthermore, the $\delta(CH)_{Py}$ bands (highlighted in yellow in Figure 2 a–e) around 770 cm^{-1} are sensitive to the occupancy of the $d_{x^2-y^2}$ orbital, as evident from the comparison of iron-oxo complexes **3**, **3**·H_2O, and **4** with different $d_{x^2-y^2}$ orbital occupancies (Figure 2 c–e). The positions of the $\delta(CH)_{Py}$ bands in **1** match those of the iron(III)-oxo complexes **3** and **3**·H_2O, thus indicating single occupancy of the $d_{x^2-y^2}$ orbital (in line with the density-functional-theory predictions, Figure S3). The presence of one electron in the $d_{x^2-y^2}$ orbital and the Co–O bond order of less than two clearly indicate that the electronic configuration of **1** is quintet.

The quintet-state assignment is further supported by comparing the visPD spectrum of **1** (430 nm–650 nm; Figure S4 a) with time-dependent DFT (TD-DFT) predictions. The visPD spectrum of **1** shows only a small absorption in the lowest experimentally accessible wavelength range, indicating an electronic transition with a maximum below 430 nm. TD-DFT predicts that the singlet and triplet states of **1** have their π*(Co–O)→π*(pyridine) transitions in the 500–650 nm range, and these transitions are shifted below 400 nm in ^{5}**1**. Therefore, the experimental visPD spectrum rules out the singlet and triplet states and thus suggests that **1** is formed as a quintet. Multireference RASPT2 and MCPDFT calculations corroborate this spin-state assignment with the quintet state being at least 15 kcal mol^{-1} more stable than the triplet and singlet states in all calculations (see the Supporting Information). The dominant RASPT2 configuration (83 %) is $(d_{xy})^2(d_{xz})^1(d_{yz})^1(d_{z^2})^1(d_{x^2-y^2})^1$ in which d_{xz}/d_{yz} are π*(Co–O) orbitals, d_{z^2} is the σ*(Co–O) orbital, and $d_{x^2-y^2}$ is the σ*(Co-ligand) orbital (Figure S5, left panel). In conclusion, IRPD and visPD spectra and theoretical calculations jointly suggest the quintet spin state of **1**.

Subsequently, we characterized the cobalt(IV)-oxo complex **2**. We have identified the Co–O vibration in the IR range below 660 cm^{-1}. The ^{18}O labeling did not only affect one band, but two: the bands at 659 cm^{-1} and 637 cm^{-1} shifted to 648 and 623 cm^{-1}. This suggests a coupling between two vibrational modes similar to what was observed in some iron-oxo complexes.[42] Here, it affects the coupling between the ν(Co–O) vibration and δ(C–N*) ligand vibration (Figure S6; N* denotes the nitrogen *trans* to the Co–O unit). The uncoupled δ(C–N*) band should be at about 644 cm^{-1}, as found for the analogous iron complex **4** (see Figure 2 e). The coupled band with a dominant δ(C–N*) contribution is at 637 cm^{-1} and

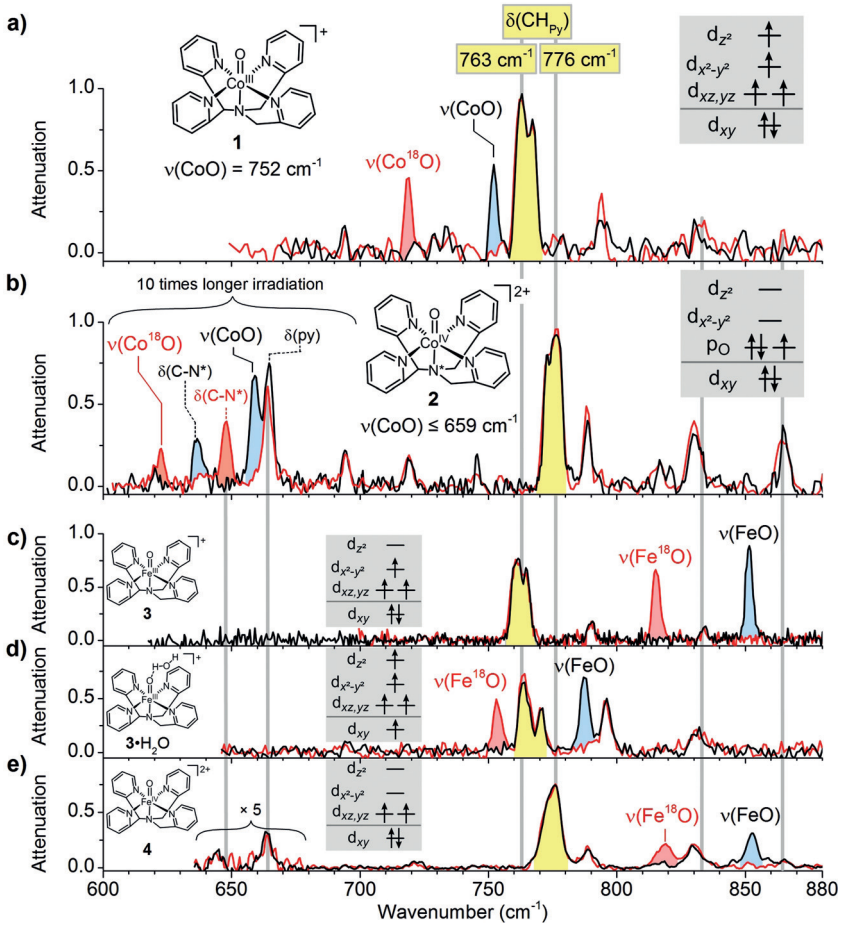

Figure 2. Infrared photodissociation spectra of complexes **1** (a), **2** (b), **3** (c), **3**·H_2O (d), and **4** (e). Black and red traces correspond to ^{16}O and to ^{18}O isotopomers, respectively. Spectra in (c–e) are taken from Refs. [32] and [44] and are shown for comparison. Grey panels show the assigned electronic configurations. In panel (b), N* denotes the nitrogen *trans* to the Co–O unit. The $\delta(CH)_{Py}$ bands are highlighted in yellow. Please note that the bands denoted as ν(Co–O) and δ(C–N*) are mixed and the denoted absorption features correspond to those where the contribution of each individual component is dominant.

shifts to 648 cm^{-1} upon the labeling. The band with the dominant ν(Co–O) contribution is at 659 cm^{-1} and shifts to 623 cm^{-1}. Hence, the uncoupled Co–O stretching frequency would be expected between 659 cm^{-1} and 636 cm^{-1}. This value implies that complex **2** features an exceptionally weak Co–O bond.

The ligand bands in the IRPD spectrum of **2** resemble those in the spectrum of iron(IV)-oxo complex **4** (see Figure 2b,e). The $\delta(CH)_{Py}$ bands are found around 775 cm^{-1} in **2**, similarly as in **4**, thus indicating that the $d_{x^2-y^2}$ orbital is unoccupied, which is compatible only with a doublet state in **2**. Furthermore, the IRPD spectrum excludes the possibility of ligand oxidation and/or de-coordination of pyridine ligand arms. Such structural modifications would result in new ligand bands in the IR spectrum (Figure S7) compared with the spectrum of **4**, which was not observed. We tried to further support the doublet spin-state assignment of **2** by visPD spectroscopy. However, the doublet and quartet states of **2** have rather similar theoretical TD-DFT spectra showing weak π*(Co–O)→σ*(Co-ligand) transitions at 550 and 520 nm, respectively. The quintet state has an intense d_{xy}-(Co)→π*(py) transition with a maximum at 420 nm. The visPD spectrum of **2** shows a peak with a shoulder at 490 nm that seems to grow in intensity, but the poor signal-to-noise ratio did not allow us to assign any particular spin state. Therefore, we turned to multireference calculations to corroborate the doublet state and to explain the very weak Co–O bond.

RASPT2 and MCPDFT calculations predict the ground state of **2** as doublet, with the quartet state being 3.3 (RASPT2) and 12.8 kcal mol^{-1} (MCPDFT) higher in energy (Table S1). The sextet state is more than 16 kcal mol^{-1} higher in energy in all calculations and is thus not further analyzed. Analysis of the RASPT2 wavefunctions of **2** in different multiplicities helps to explain the weak Co–O bond and to discard the quartet state of **2** as the ground state. The dominant configuration (80%) in the quartet state of **2** in these calculations is similar to the configuration of iron(III)-oxo complex **3**, that is, $(d_{xy})^2(d_{xz})^1(d_{yz})^1(d_{x^2-y^2})^1(d_{z^2})^0$, wherein d_{xz}/d_{yz} are the π*(Co–O) orbitals, $d_{x^2-y^2}$ is the σ*(Co-ligand) orbital, and d_{z^2} is the σ*(Co–O) orbital. Thus, the Co–O bond strength in the quartet state of **2** should be similar to that in **3**. However, the Co–O stretching frequency in **2** is almost 200 cm^{-1} lower than that of **3** (ν(Fe–O) = 851 cm^{-1}).[32] Thus,

the low Co–O bond strength is inconsistent with the electronic configuration of the quartet state of **2**.

The doublet-state configuration of **2** is unlike any configuration observed in iron-oxo complexes thus far, because the cobalt d orbitals lie lower in energy than the oxygen p orbitals (Figure S5). The bonding π(Co–O) orbitals are now dominantly Co-based d orbitals, while the antibonding π*(Co–O) orbitals are O-based p orbitals. Therefore, the frontier molecular orbitals are no longer cobalt-based but instead oxygen-based, with the electronic configuration being $(d_{xy})^2(p_x(O))^2(p_y(O))^1(d_{z^2})^0(d_{x^2-y^2})^0$. Thus, the bonding situation in the doublet complex **2** is best formulated as the Co^{III} center bound to the oxyl group ($O^{\bullet-}$) with the unpaired electron in a p orbital perpendicular to the Co–O axis. This cobalt(III)-oxyl bonding with a shallow Co–O potential (Figure S9) is consistent with the low experimentally observed ν(Co–O) stretching frequency. Markedly, the frequency of the ν(Co–O) vibration in **2** is even lower than in the $[(L)CuO]^+$ complexes (L = CH_3CN, phen, 1,10-phenanthrenequinone), where the metal-oxo bonding varies between copper(I)-oxygen ($Cu^IO^{\bullet\bullet}$) and copper(II)-oxyl ($Cu^{II}O^{-\bullet}$) configurations, depending on the ligand.[43] This showcases the highly destabilizing effect of the tetragonal environment on the metal-oxo bonding in **2**. In conclusion, the low-frequency ν(Co–O) vibration, the characteristic ligand vibrations, and the multireference calculations indicate that the ground spin state of **2** is doublet. We note that while all experimental and theoretical results are consistent and indicate the same spin assignments, none of the experimental results shows the spin state of the investigated complexes directly. Therefore, corroborating measurements such as EPR spectroscopy would be desirable once it is possible to prepare these complexes in the condensed phase.

To probe the chemical reactivity of **1** and **2**, we measured their gas-phase reactivity (details in the Supporting Information). We tested their reactivity with 1,4-cyclohexadiene, which reacts with iron(IV)-oxo complexes by hydrogen atom transfer (HAT) or hydride transfer,[44,38] and with ethanethiol, which reacts with iron(III)-oxo complexes by proton-coupled electron transfer (PCET).[32]

Surprisingly, complex **1** was completely unreactive towards both 1,4-cyclohexadiene and ethanethiol. This suggests that the occupancy of the d_{z^2} orbital prohibits the low-energy σ pathway for HAT typically observed for iron(IV)-oxo complexes.[45,46] In iron(IV)-oxo complexes, the incoming electron from the hydrogen atom goes into the unoccupied d_{z^2} orbital and forms a high-spin sextet transition state with oxyl radical character. On the contrary, an electron incoming to **1** would have to go into an already occupied orbital, which is energetically less favored. Furthermore, the lack of PCET reactivity with ethanethiol implies that the basicity of cobalt(III)-oxo complex **1** is lower than that of **3** and of all other gaseous iron(III)-oxo complexes reported in Ref. [32].

Conversely, complex **2** reacts with 1,4-cyclohexadiene very efficiently via HAT (Figure 3a). Using partially deuterated 1,4-cyclohexadiene-1,2,3,4,5,6-d_6,[38] we determined the intramolecular kinetic isotope effect (KIE) of the HAT reaction to be 2.1 ± 0.1, which falls below the KIEs observed in iron(IV)-oxo complexes.[44] The measured KIE is in fact in

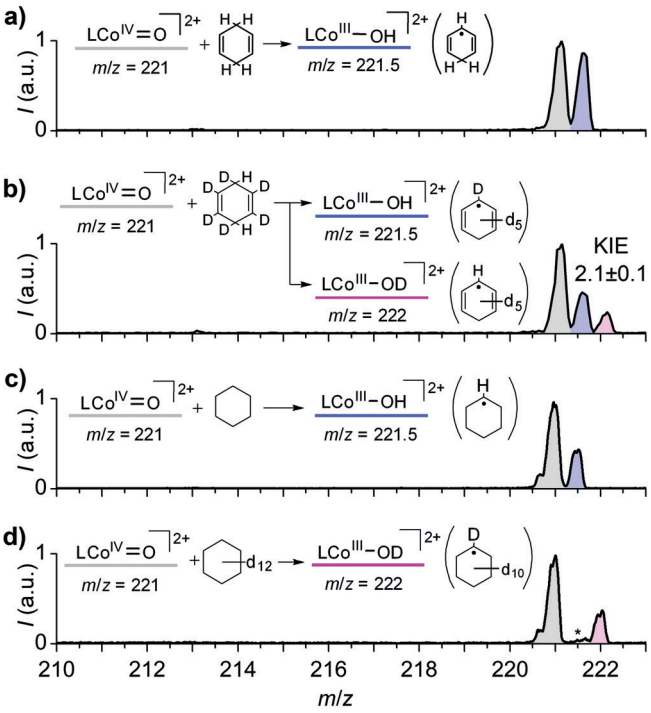

Figure 3. Gas-phase reactivity of **2** (p = 0.2 mTorr) with a) 1,4-cyclohexadiene, b) 1,4-cyclohexadiene-1,2,3,4,5,6-d_6, c) cyclohexane and d) cyclohexane-d_{12}. Corresponding neutral products are given in parentheses. Reactions were measured at nominally zero-collision energy determined from the retarding potential analysis (Figure S10). The peak at m/z = 221.5 in (d) denoted with an asterisk results from reactions with impurities in the collision cell. With cyclohexane, we observed a subsequent addition of mass 144 from an unidentified impurity to the HAT reaction products, which could not be eliminated.

the range observed in HAT reactions mediated by highly reactive small model metal-oxo cations.[47] Consistently, we found that **2** is also capable of hydrogen-atom abstraction from a non-activated alkane, in this case cyclohexane (Figure 3c,d, C–H bond dissociation energy: 99.5 kcal mol^{-1} [48]). Activation of strong secondary C–H bonds in a single collision experiment in the gas phase has only been reported for bare metal or metal-oxo ions, or for coordinatively unsaturated, highly reactive species such as $[(phen)Cu(O)]^+$ so far, because the reaction must be barrierless with respect to the separated reactants to occur.[49–51] Even high-valent non-heme iron(IV)-oxo and iron(V)-oxo complexes, readily reactive towards these C–H bonds in solution, are unreactive in the gas phase. We have also probed the activation of a primary C–H bond in ethane, which was not observed (k_{rel}(ethane/cyclohexane) < 0.02), and the reaction with water,[40] which did not occur either. In conclusion, complex **2** is a strong hydrogen-atom abstractor capable to react with non-activated secondary C–H bonds.

To corroborate the exceptionally high reactivity of **2**, we performed exploratory DFT calculations of the HAT reaction between **2** and the secondary C–H group of propane, a model of a cyclohexane methylene group. The DFT calculations showed that the reaction occurs entirely on the doublet potential energy surface (Figure 4). The reaction proceeds with a π*-approach trajectory enforced by the π*-oxyl radical

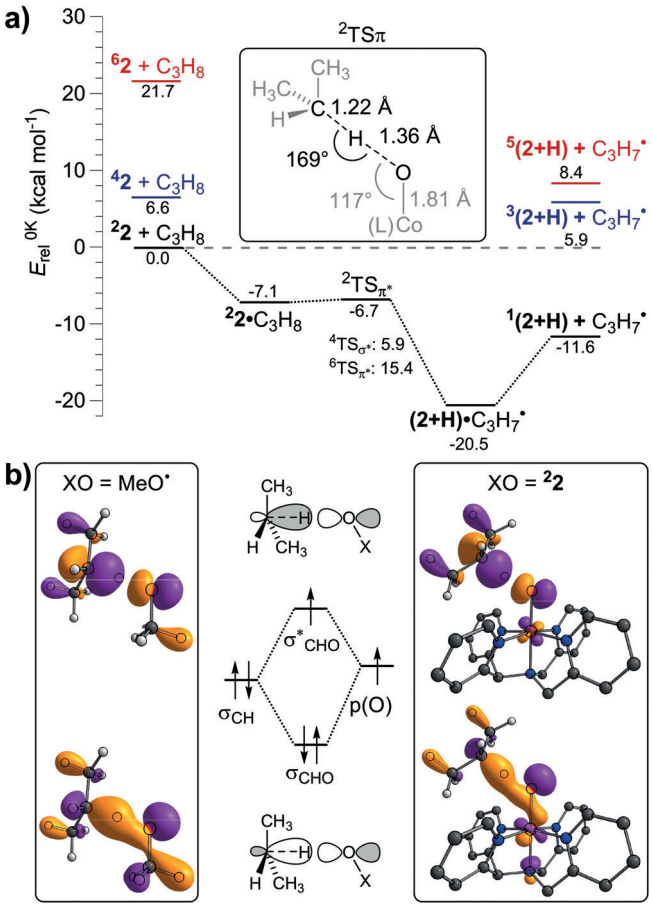

Figure 4. a) B3LYP-D3/6-311+G** potential energy profile for the reaction of **2** with the secondary hydrogen of propane. b) Schematic representation of the molecular orbitals involved in the HAT reaction of propane with the methoxy radical (left) and ^{2}**2** (right; ligand hydrogens have been omitted for clarity). The Kohn–Sham orbitals correspond to the α(HOMO) and β(HOMO−1) orbitals at the transition states (see also Figure S8).

in ^{2}**2** (α(Co-O-H) = 117°) and has a small energy barrier (0.4 kcal mol^{-1}) with respect to the reactant complex. The reaction pathway resembles a C–H activation by a free methoxy radical and thus corresponds to a direct abstraction of the hydrogen atom by the oxyl radical (Figure 4b).[52] The reaction pathway is in contrast with the reactivity of iron(IV)-oxo compounds in which the oxyl radical only develops upon Fe=O bond elongation during the substrate approach.[53,54]

Conclusion

In summary, we reported the generation and characterization of terminal cobalt(III)-oxo (**1**) and cobalt(IV)-oxo (**2**) complexes in pseudo-tetragonal geometry with the N4Py ligand. Both these tetragonal Group-9 complexes feature more than five d electrons and can thus be considered to be behind the oxo wall. Contrary to our initial expectations, complex **1** has a cobalt-oxo bond of similar strength to sextet iron(III)-oxo complexes (ν(Co–O) = 752 cm^{-1}) and is unreactive towards C–H and S–H bonds. Conversely, complex **2** features a very weak cobalt-oxyl bond (ν(Co–O) ≤ 659 cm^{-1}) and abstracts a hydrogen atom from cyclohexane. Such a reactivity has only been previously reported for coordinatively unsaturated gaseous metal-oxo model complexes undetected in solution. However, coordinatively saturated complexes, such as **2**, could potentially be prepared in the condensed phase,[55] which would also enable their definitive characterization. Therefore, they are promising targets for developing highly active C–H oxidation catalysts.

Acknowledgements

The project was funded by the European Research Council (ERC CoG No. 682275), the Czech Ministry of Education, Youth and Sports (LTAUSA17026), the COST action ECOSTBio, MINECO of Spain (CTQ2015-70795-P), the Catalan DIUE of the Generalitat de Catalunya (2017SGR01378, a BFI PhD grant to M.R., and an ICREA-Academia award), and the Grant Agency of the Czech Republic (Grant No. 18-13093S). We thank Carlos V. Melo for proofreading the manuscript.

Conflict of interest

The authors declare no conflict of interest.

Stichwörter: C-H-Aktivierung · Cobalt-Oxo-Komplexe · Eisen-Oxo-Komplexe · Helium-Tagging · Ionenspektroskopie · Oxo-Mauer

Zitierweise: *Angew. Chem. Int. Ed.* **2019**, *58*, 9619–9624
Angew. Chem. **2019**, *131*, 9721–9726

[1] C. J. Ballhausen, H. B. Gray, *Inorg. Chem.* **1962**, *1*, 111–122.
[2] J. R. Winkler, H. B. Gray, *Struct. Bonding (Berlin)* **2012**, *142*, 17–28.
[3] *Cytochrome P450: Structure, Mechanism, and Biochemistry*, 3rd ed. (Ed.: P. R. Ortiz de Montellano), Kluwer Academic/Plenum Press, New York, **2005**.
[4] F. P. Guengerich, *ACS Catal.* **2018**, *8*, 10964–10976.
[5] X. Huang, J. T. Groves, *Chem. Rev.* **2018**, *118*, 2491–2553.
[6] M. M. Abu-Omar, A. Loaiza, N. Hontzeas, *Chem. Rev.* **2005**, *105*, 2227–2252.
[7] E. I. Solomon, T. C. Brunold, M. I. Davis, J. N. Kemsley, S.-K. Lee, N. Lehner, F. Neese, A. J. Skulan, Y.-S. Yang, J. Zhou, *Chem. Rev.* **2000**, *100*, 235–349.
[8] J. Hohenberger, K. Ray, K. Meyer, *Nat. Commun.* **2012**, *3*, 720.
[9] A. C. Lindhorst, S. Haslinger, F. E. Kühn, *Chem. Commun.* **2015**, *51*, 17193–17212.
[10] „Biomimetic High-Valent Mononuclear Nonheme Iron-Oxo Chemistry“: J. E. M. N. Klein, L. Que, Jr. in *Encyclopedia of Inorganic and Bioinorganic Chemistry* (Ed.: R. A. Scott), Wiley, Chichester, **2016**.
[11] B. Wang, Y.-M. Lee, W.-Y. Tcho, S. Tussupbayev, S.-T. Kim, Y. Kim, M. S. Seo, K.-B. Cho, Y. Dede, B. C. Keegan, T. Ogura, S. H. Kim, T. Ohta, M.-H. Baik, K. Ray, J. Shearer, W. Nam, *Nat. Commun.* **2017**, *8*, 14839.
[12] M. K. Goetz, E. A. Hill, A. S. Filatov, J. S. Anderson, *J. Am. Chem. Soc.* **2018**, *140*, 13176–13180.

[13] R. S. Hay-Motherwell, G. Wilkinson, B. Hussain-Bates, M. B. Hursthouse, *Polyhedron* **1993**, *12*, 2009 – 2012.
[14] E. Poverenov, I. Efremenko, A. I. Frenkel, Y. Ben-David, L. J. W. Shimon, G. Leitus, L. Konstantinovski, J. M. L. Martin, D. Milstein, *Nature* **2008**, *455*, 1093 – 1096.
[15] S. Hong, F. F. Pfaff, E. Kwon, Y. Wang, M.-S. Seo, E. Bill, K. Ray, W. Nam, *Angew. Chem. Int. Ed.* **2014**, *53*, 10403 – 10407; *Angew. Chem.* **2014**, *126*, 10571 – 10575.
[16] K. P. O'Halloran, C. Zhao, N. S. Ando, A. J. Schultz, T. F. Koetzle, P. M. B. Piccoli, B. Hedman, K. O. Hodgson, E. Bobyr, M. L. Kirk, S. Knottenbelt, E. C. Depperman, B. Stein, T. M. Anderson, R. Cao, Y. V. Geletii, K. I. Hardcastle, D. G. Musaev, W. A. Neiwert, X. Fang, K. Morokuma, S. Wu, P. Kogerler, C. L. Hill, *Inorg. Chem.* **2012**, *51*, 7025 – 7031.
[17] J. M. Mayer, *Comments Inorg. Chem.* **1988**, *8*, 125 – 135.
[18] R. H. Holm, *Chem. Rev.* **1987**, *87*, 1401 – 1449.
[19] H. B. Gray, J. R. Winkler, *Acc. Chem. Res.* **2018**, *51*, 1850 – 1857.
[20] S. Mukerjee, K. Skogerson, S. DeGala, J. P. Caradonna, *Inorg. Chim. Acta* **2000**, *297*, 313 – 329.
[21] K. Ray, F. Heims, F. F. Pfaff, *Eur. J. Inorg. Chem.* **2013**, 3784 – 3807.
[22] M. Shelef, *Chem. Rev.* **1995**, *95*, 209 – 225.
[23] D. Das, S. Pattanayak, K. K. Singh, B. Garaib, S. S. Gupta, *Chem. Commun.* **2016**, *52*, 11787 – 11790.
[24] L. Nurdin, D. M. Spasyuk, L. Fairburn, W. E. Piers, L. Maron, *J. Am. Chem. Soc.* **2018**, *140*, 16094 – 16105.
[25] A. I. Ngyuen, R. G. Hadt, E. I. Solomon, D. Tilley, *Chem. Sci.* **2014**, *5*, 2874 – 2878.
[26] M. W. Kanan, Y. Surendranath, D. G. Nocera, *Chem. Soc. Rev.* **2009**, *38*, 109 – 114.
[27] A. I. Nguyen, M. S. Ziegler, P. Oña-Burgos, M. Sturzbecher-Hohne, W. Kim, D. E. Bellone, T. D. Tilley, *J. Am. Chem. Soc.* **2015**, *137*, 12865 – 12872.
[28] E. Spaltenstein, R. R. Conry, S. C. Critchlow, J. M. Mayer, *J. Am. Chem. Soc.* **1989**, *111*, 8741 – 8742.
[29] C. E. MacBeth, A. P. Golombek, V. G. Young, C. Yang, K. Kuczera, M. P. Hendrich, A. S. Borovik, *Science* **2000**, *289*, 938 – 941.
[30] J. M. Smith, D. E. Mayberry, C. G. Margarit, J. Sutter, H. Wang, K. Meyer, R. P. Bontchev, *J. Am. Chem. Soc.* **2012**, *134*, 6516 – 6519.
[31] E. M. Matson, Y. J. Park, A. R. Fout, *J. Am. Chem. Soc.* **2014**, *136*, 17398 – 17401.
[32] E. Andris, R. Navrátil, J. Jašík, M. Puri, M. Costas, L. Que, Jr., J. Roithová, *J. Am. Chem. Soc.* **2018**, *140*, 14391 – 14400.
[33] J. E. House, *Inorganic Chemistry*, 2nd ed., Academic Press, New York, **2013**, pp. 591 – 616.
[34] D. Schröder, H. Schwarz, *Proc. Natl. Acad. Sci. USA* **2008**, *105*, 18114 – 18119.
[35] J. Roithová, A. Gray, E. Andris, J. Jašík, D. Gerlich, *Acc. Chem. Res.* **2016**, *49*, 223 – 230.
[36] L. Jašíková, J. Roithová, *Organometallics* **2012**, *31*, 1935 – 1942.
[37] J. Jašík, D. Gerlich, J. Roithová, *J. Phys. Chem. A* **2015**, *119*, 2532 – 2542.
[38] E. Andris, J. Jašík, L. Gómez, M. Costas, J. Roithová, *Angew. Chem. Int. Ed.* **2016**, *55*, 3637 – 3641; *Angew. Chem.* **2016**, *128*, 3701 – 3705.
[39] D. Schröder, J. Roithová, H. Schwarz, *Int. J. Mass Spectrom.* **2006**, *254*, 197 – 201.
[40] G. Yassaghi, E. Andris, J. Roithová, *ChemPhysChem* **2017**, *18*, 2217 – 2224.
[41] A. Call, C. Casadevall, F. Acuña-Parés, A. Casitas, J. Lloret-Fillol, *Chem. Sci.* **2017**, *8*, 4739 – 4749.
[42] J. England, J. Prakash, M. A. Cranswick, D. Mandal, Y. Guo, E. Münck, S. Shaik, L. Que, Jr., *Inorg. Chem.* **2015**, *54*, 7828 – 7839.
[43] M. Srnec, R. Navrátil, E. Andris, J. Jašík, J. Roithová, *Angew. Chem. Int. Ed.* **2018**, *57*, 17053 – 17057; *Angew. Chem.* **2018**, *130*, 17299 – 17303.
[44] E. Andris, R. Navrátil, J. Jašík, T. Terencio, M. Srnec, M. Costas, J. Roithová, *J. Am. Chem. Soc.* **2017**, *139*, 2757 – 2765.
[45] S. Ye, C.-Y. Geng, S. Shaik, F. Neese, *Phys. Chem. Chem. Phys.* **2013**, *15*, 8017 – 8030.
[46] D. Janardanan, Y. Wang, P. Schyman, L. Que, Jr., S. Shaik, *Angew. Chem. Int. Ed.* **2010**, *49*, 3342 – 3345; *Angew. Chem.* **2010**, *122*, 3414 – 3417.
[47] H. Schwarz, *Angew. Chem. Int. Ed.* **2011**, *50*, 10096 – 10115; *Angew. Chem.* **2011**, *123*, 10276 – 10297.
[48] Y. R. Luo, *Comprehensive Handbook of Chemical Bond Energies*, CRC Press, Taylor & Francis Group, Boca Raton, FL, **2007**.
[49] J. Roithová, D. Schröder, *Chem. Rev.* **2010**, *110*, 1170 – 1211.
[50] D. Schröder, M. C. Holthausen, H. Schwarz, *J. Phys. Chem. B* **2004**, *108*, 14407 – 14416.
[51] G. Yassaghi, E. Andris, J. Roithová, *ChemPhysChem* **2017**, *18*, 2217 – 2224.
[52] B. Mondal, L. Roy, F. Neese, S. Ye, *Isr. J. Chem.* **2016**, *56*, 763 – 772.
[53] S. Ye, F. Neese, *Proc. Natl. Acad. Sci. USA* **2011**, *108*, 1228 – 1233.
[54] M. Srnec, S. D. Wong, J. England, L. Que, Jr., E. I. Solomon, *Proc. Natl. Acad. Sci. USA* **2012**, *109*, 14326 – 14331.
[55] R. Zhang, M. Newcomb, *Acc. Chem. Res.* **2008**, *41*, 468 – 477.

Manuskript erhalten: 12. April 2019
Veränderte Fassung erhalten: 13. Mai 2019
Akzeptierte Fassung online: 13. Mai 2019
Endgültige Fassung online: 11. Juni 2019

